AN OPTIMIZATION APPROACH TO UNCERTAINTY PROPAGATION IN BOUNDARY LOAD FLOW

Andrija T. Sarić
Northeastern University
Boston, Massachusetts
asaric@tfc.kg.ac.yu

Branko Glišović
Northeastern University
Boston, Massachusetts
glisovic@ece.neu.edu

Aleksandar M. Stanković
Northeastern University
Boston, Massachusetts
astankov@ece.neu.edu

Abstract – Boundary load flow exemplifies a class of power (load) flow models that explicitly incorporates uncertainties in system data. Its importance for operation and control of modern power systems is increasing due to changes in ways the system is operated following deregulation and due to the emergence of new types of sources (e.g., distributed generation). Modeling based on interval computations is a rigorous mathematical tool for worst-case analysis of uncertain systems. This paper proposes an optimization-based approach to minimizing uncertainty spread in a boundary load flow model. The approach combines interval computations with a linear programming-based heuristic that is effective in avoiding the excessive conservativism often associated with direct interval computations. We consider the case of uncertainty in both measurements (e.g., SCADA) and network parameters. The method is potentially applicable to large-scale power systems, and we study its performance on a two benchmark examples: New England/New York interconnection with 68 nodes and standard IEEE test system with 300 nodes.

Keywords *– Power flow analysis, Uncertainty, Optimization methods.*

1 INTRODUCTION

Several types of uncertainty affect the practical feasibility of real-time power flow calculations: 1) topological uncertainties, 2) uncertainty in network parameters, and 3) possible errors in measurements (e.g., SCADA). Topological uncertainties are linked with the fidelity of signalization and unexpected outages of power system elements. These are typically large discrepancies, and in this paper we assume that they have been handled properly, so the topology of the network is exactly known. On the other hand, errors in network parameters and in SCADA measurements tend to be smaller in size, but harder to detect in practice. Analogous problems persist in power flow calculations based on forecasted data.

This paper studies the effects of network parameter and measurement uncertainties. The propagation of these "input" uncertainties through power system calculations is often very complex, due for example to inversions of uncertain matrices like Jacobians. Different approaches have been suggested in the literature as ways to quantify the uncertainty propagation in power flow: a) parametric and sensitivity based methods [1], [2], b) probabilistic methods [3], [4], c) interval and fuzzy calculations [5], [6], and d) boundary load flow framework [7]. These methods determine distribution of power flow solutions and/or bounding between extreme (pessimistic and optimistic) solutions.

Utility experience, as well as Monte Carlo simulations (which serve as standard tool for verification of various methods) suggests that critical situations (with largest uncertainty spread) are very rare. The spread between extreme and the most likely results builds up quickly with the increase in problem (system) size. This, however, does not diminish the importance of understanding the implications of worst-case scenarios, as recent experiences with blackouts clearly show.

This paper presents a power flow analysis model that includes uncertainties in input data (SCADA measurements and network parameters) in an exact, rigorous mathematical way. The model is based on interval arithmetic analysis combined with linear programming, which performs maximization of interval widths to determine the worst cases. The original optimization model with interval values of cost function and of equality constraints is transformed into a standard linear programming (LP) formulation with deterministic cost function and pairs of non-interval inequality constraints. Our methodology predicts variations in nodal (magnitude, angle) and line (power flow) quantities caused by model and measurement uncertainties. While to some degree conservative, our results are much tighter than those obtained by direct application of interval computation methods. At the same time, our results are rigorous worst-case predictions, and as such may prove useful in operation and control of power systems. While our current implementation is intended for off-line analyses, we feel that alterations (e.g., with a state-of-the-art LP software like GAMS) would make it capable of solving systems with a few thousand variables in an online environment.

The rest of the paper is organized as follows – in *Section 2* we formulate the problem of interval load flow in detail, following solution by optimization method described in *Sections 3* and *4*; in *Section 5* we apply proposed methods to two benchmark power systems (the first is New England/New York 68 nodes/86 lines, and the second is the IEEE benchmark with 300 nodes/411 lines), followed by brief conclusions in *Section 6*. The *Appendix* contains equations used to model the power system.

2 BOUNDARY INTERVAL LOAD FLOW (BILF) FORMULATION

The general form of power flow equations with interval variables is given by:

$$\boldsymbol{g}(\boldsymbol{X},\boldsymbol{Y}_b^c)=\boldsymbol{b}; \quad (1)$$

$$\boldsymbol{h}_S(\boldsymbol{X},\boldsymbol{b},\boldsymbol{Y}_b^c)=\boldsymbol{S}_b^c, \quad (2)$$

where:

$\boldsymbol{X}=[\underline{\boldsymbol{X}};\overline{\boldsymbol{X}}]$ – vector of unknown interval state variables (voltage angles in PQ and PV nodes, voltage magnitudes in PQ nodes, and reactive powers in PV nodes, or $\boldsymbol{X}=[\boldsymbol{\theta}_{PQ+PV}\ \ \boldsymbol{V}_{PQ}\ \ \boldsymbol{Q}_{PV}]^{\mathrm{T}}$);

$\boldsymbol{Y}_b^c=[\underline{\boldsymbol{Y}}_b^c;\overline{\boldsymbol{Y}}_b^c]$ – vector of network interval branch (lines and transformers) admittances, or $\boldsymbol{Y}_b^c=\boldsymbol{G}_b+j\boldsymbol{B}_b$;

$\boldsymbol{b}=[\underline{\boldsymbol{b}};\overline{\boldsymbol{b}}]$ – vector of SCADA measured (or forecasted) input interval variables (real injections in PQ and PV nodes, reactive injections in PQ nodes, and voltage magnitudes in PV nodes, or $\boldsymbol{b}=[\boldsymbol{P}_{PQ+PV}\ \ \boldsymbol{Q}_{PQ}\ \ \boldsymbol{V}_{PV}]^{\mathrm{T}}$);

$\boldsymbol{S}_b^c=[\underline{\boldsymbol{S}}_b^c;\overline{\boldsymbol{S}}_b^c]$ – vector of unknown output interval MVA complex variables (real and reactive power flows in branches, or $\boldsymbol{S}_b^c=\boldsymbol{P}_b+j\boldsymbol{Q}_b$);

$\boldsymbol{g}$, $\boldsymbol{h}_S$ – node injection and MVA branch flow functions, respectively;

$\underline{\ }$, $\overline{\ }$ – lower and upper interval bounds, respectively;

^{c} – superscript denotes complex variable.

The detailed versions of (1) and (2) are given in *Appendix*. The flow-chart of BILF is shown in Figure 1.

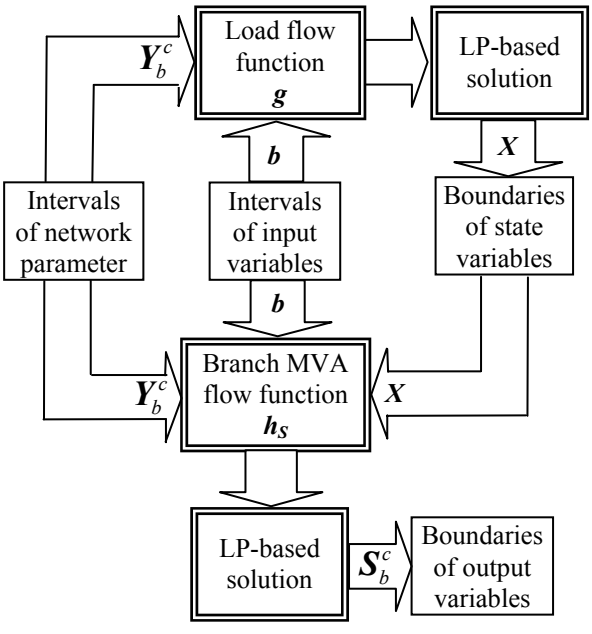

Figure 1: The flow-chart of BILF.

3 LP-BASED SOLUTION OF INTERVAL EQUATIONS

A general *n*-dimensional system of linear interval equations can be formulated as:

$$\boldsymbol{A}\boldsymbol{X}=\boldsymbol{b}, \quad (3)$$

with lower/upper bound constraints:

$$\boldsymbol{X}_{\min}\le\boldsymbol{X}\le\boldsymbol{X}_{\max}, \quad (4)$$

where: $\boldsymbol{A}=[\underline{\boldsymbol{A}};\overline{\boldsymbol{A}}]$, $\boldsymbol{X}=[\underline{\boldsymbol{X}};\overline{\boldsymbol{X}}]$ and $\boldsymbol{b}=[\underline{\boldsymbol{b}};\overline{\boldsymbol{b}}]$.

System of equations (3)–(4) can be re-formulated as an linear programming (LP) problem, with the aim to maximize the width of an interval solution [8]:

$$\max\sum_{j=1}^{n}\left(\overline{X}_j-\underline{X}_j\right), \quad (5)$$

subject to interval equality constraints:

$$\sum_{j=1}^{n}A_{ij}X_j=b_i;\ i=1,2,\cdots,n. \quad (6)$$

and lower/upper interval bound constraints (minimal deviation of intervals from middle point solution):

$$X_{j,\min}\le\underline{X}_j\le X_m\le\overline{X}_j\le X_{j,\max};\ j=1,2,\cdots,n. \quad (7)$$

An interval equality constraint (6) can be re-formulated as the following pair of non-interval constraints:

- $$\sum_{j=1}^{n}A_{ij}^{''}X_j^{''}\le\overline{b}_i;\ i=1,2,\cdots,n, \quad (8)$$

  where:

  $$A_{ij}^{''}=\underline{A}_{ij};\ X_j^{''}=\underline{X}_j,\quad \textit{iff}\ \ \underline{X}_j\ge 0;$$

  $$A_{ij}^{''}=\overline{A}_{ij};\ X_j^{''}=\overline{X}_j,\quad \textit{iff}\ \ \overline{X}_j\le 0.$$

- $$\sum_{j=1}^{n}A_{ij}^{'}X_j^{'}\ge\underline{b}_i;\ i=1,2,\cdots,n, \quad (9)$$

  where:

  $$A_{ij}^{'}=\overline{A}_{ij};\ X_j^{'}=\overline{X}_j,\quad \textit{iff}\ \ \underline{X}_j\ge 0;$$

  $$A_{ij}^{'}=\underline{A}_{ij};\ X_j^{'}=\underline{X}_j,\quad \textit{iff}\ \ \overline{X}_j\le 0.$$

The algorithmic solution of the LP problem (5)–(9) is enumerative: we need to solve the model twice, once with assumption that $\underline{X}_j\ge 0$, and once with the assumption that $\overline{X}_j\le 0$, and choose the version yielding the optimum of interest. Then, for $j=1,2,\cdots,n$ it will require 2^n solutions for each optimum of interest. This number increases exponentially, which is not accept-

able for realistic power systems. For this reason, we use the following heuristic: calculate non-interval (middle-point) solution, and then with calculated and *fixed signs* for X_j evaluate their corresponding intervals.

Given our desire to calculate non-conservative, tight intervals widths, it is critical that calculation both left-side matrix $\boldsymbol{A}$ and right-side vector $\boldsymbol{b}$ be based on realistic bounds. In the power system case, their variations are additionally constrained. For example, in submatrix $\frac{\partial \boldsymbol{P}_{PQ+PV}}{\partial \boldsymbol{\theta}_{PQ+PV}}$ in (A1) all diagonal elements are approximately equal to the negative sum of off-diagonal elements. This means that various entries should not be treated as mutually independent, as commonly assumed in interval solvers [9], [10]. The additional constraints can be conveniently handled with the row-based LP-approach from (5)–(9).

4 MAXIMIZED BILF MODEL

The solution of load flow equations (1) by standard interval analysis tools (such as interval matrix inversion [9], different contractors [10], direct application of interval computations [5], etc.) gives very wide interval variables, rendering inconsequential for industrial applications.

Starting with linearized power flow equations (1) we can reformulate the problem in the form:

$$\boldsymbol{J}\bullet\Delta\boldsymbol{X}=\boldsymbol{J}\bullet(\boldsymbol{X}-\boldsymbol{X}_m)=\boldsymbol{b}-\boldsymbol{b}_m=\Delta\boldsymbol{b}, \qquad (10a)$$

or:

$$\boldsymbol{J}\bullet\boldsymbol{X}=\boldsymbol{b}', \qquad (10b)$$

where $\boldsymbol{J}=[\underline{\boldsymbol{J}};\overline{\boldsymbol{J}}]$ is interval Jacobian matrix defined on basis eq. (A1), $\boldsymbol{b}'=\boldsymbol{b}-\boldsymbol{b}_m+\boldsymbol{J}\bullet\boldsymbol{X}_m$ and subscript $_m$ denotes variables in the middle point of interval. The interval Jacobian matrix $\boldsymbol{J}$ is calculated for intervals of network parameters $\boldsymbol{Y}_b^c$ and middle point values ($\boldsymbol{X}_m$) of unknown interval variable vector $\boldsymbol{X}=[\underline{\boldsymbol{X}};\overline{\boldsymbol{X}}]$.

For algorithm described in *Section 3*, formulation (10b) is preferred over standard formulation, as it makes the sign of interval variables equal to the sign of middle point variables. For (10b) we can apply LP-based formulation for solution of interval equations:

$$\max\sum_{j=1}^{n}k_j\frac{\overline{X}_j-\underline{X}_j}{X_m}, \qquad (11a)$$

subject to interval equality constraints:

$$\sum_{j=1}^{n}J_{ij}X_j=b_i';\ i=1,2,\cdots,n, \qquad (11b)$$

and lower and upper boundary constraints for PQ-node voltages and PV-node reactive powers, respectively:

$$\boldsymbol{V}_{PQ,\min}\le\underline{\boldsymbol{V}}_{PQ};\ \overline{\boldsymbol{V}}_{PQ}\le\boldsymbol{V}_{PQ,\max}; \qquad (11c)$$

$$\boldsymbol{Q}_{PV,\min}\le\underline{\boldsymbol{Q}}_{PV};\ \overline{\boldsymbol{Q}}_{PV}\le\boldsymbol{Q}_{PV,\max}, \qquad (11d)$$

where subscripts $_{\min}$ and $_{\max}$ denote minimum and maximum, respectively.

The coefficient k_j in (11a) aims to equalize contributions to the criterion function of various types of entries (voltage angles and magnitudes, etc.) in the state vector $\boldsymbol{X}=[\boldsymbol{\theta}_{PQ+PV}\ \ \boldsymbol{V}_{PQ}\ \ \boldsymbol{Q}_{PV}]^{\mathrm{T}}$. We found empirically that the following selection works well in simulations: $\boldsymbol{\kappa}_\theta=\boldsymbol{1}$, $\boldsymbol{\kappa}_V=N_\theta/N_V=\left(N_{PQ}+N_{PV}\right)/N_{PV}$ and $\boldsymbol{\kappa}_Q=N_\theta/N_Q=\left(N_{PQ}+N_{PV}\right)/N_{PQ}$. As expected, if the decoupled model (e.g., Stott-Alsac) is used, then $\boldsymbol{\kappa}_\theta=\boldsymbol{\kappa}_V=\boldsymbol{\kappa}_Q=\boldsymbol{1}$.

In a similar way, the initial interval branch flows $\boldsymbol{S}_b^c$ (2) are calculated (e.g., for real powers) as:

$$\boldsymbol{J}_P\bullet\boldsymbol{X}_n=\boldsymbol{P}_b', \qquad (12)$$

where $\boldsymbol{J}_P=[\underline{\boldsymbol{J}}_P;\overline{\boldsymbol{J}}_P]$ is interval branch flow sensitivity matrix (equation (A4) in *Appendix*) and $\boldsymbol{P}_b'=\boldsymbol{P}_b-\boldsymbol{P}_{bm}+\boldsymbol{J}_P\bullet\boldsymbol{X}_{nm}$. The interval sensitivity matrix $\boldsymbol{J}_P$ is calculated for intervals of network parameters $\boldsymbol{Y}_b^c$ and middle point of intervals of system node variables $\boldsymbol{X}_{nm}=[\boldsymbol{\theta}_m\ \ \boldsymbol{V}_m]^{\mathrm{T}}$. However, branch flow intervals calculated by (12) tend to be very wide, and sometimes even contradictory with the nodal power balance.

After (12) has been solved, the real power branch flows are additionally constrained with the LP-based approach:

$$\max\sum_{\ell=1}^{L_s}\left(\overline{P}_{b\ell}-\underline{P}_{b\ell}\right), \qquad (13a)$$

subject to interval inequality (branch real power flow increments with perturbation) and equality (node real load balance) constraints, respectively:

$$\sum_{j=1}^{n}J_{P,\ell j}X_{nj}\ge P_{b\ell}-P_{bm}+\boldsymbol{J}_PX_{nm};\ \ell=1,2,\cdots,L_s. \qquad (13b)$$

$$P_k+\sum_{\ell=1}^{k_\ell}\boldsymbol{P}_{b,\ell}'=0;\ k=1,2,\cdots,n_{bus}\ne n_{SL}. \qquad (13c)$$

where:

$L_s=L-L_{SL}$ (L_{SL} is set of branches connected with slack (SL) node(s));

P_k – real injections (generation, loads, compensation, shunt branch admittances) in the *k*-th node;

k_ℓ – number of braches connected with *k*-th node.

Finally, we must calculate power flows for set of branches connected with slack node(s) L_{SL}, injection(s) in slack node(s) *SL* and system losses on a direct way (without optimization).

The proposed formulation is general for full (e.g., Newton-Raphson) or decoupled (e.g., Stott-Alsac) power flow methods. In our BILF model we assume that uncertainties in network parameters and in SCADA measurements (in advance specified inputs for power flow calculations) are small enough, so that a single Jacobian can capture the behavior of the power flow solution. In particular, we use a (carefully selected – see (10b)) linearization to evaluate effects of uncertainties. If the magnitude of uncertainty is so large that this assumption is violated, then an iterative procedure may offer an improved solution; we did not pursue this path further.

5 APPLICATION

The maximized BILF model for calculation of node voltages and power flows with uncertainties in network parameters and measurement data set has been implemented in Matlab environment and tested on two standard test examples.

5.1 New England/New-York interconnection with 68 nodes

The first test system comprises 68 buses, 16 generators and 86 lines. Three of the generators (14, 15 and 16) are very large equivalents of neighboring systems.

The values for SCADA measurement vector ***b*** (real loads in (PQ + PV)-nodes, reactive loads in PQ-nodes, real generations in PV-nodes and voltage magnitudes in PV-nodes) and network branch parameter vector ($\boldsymbol{Y}_b^c$) are uncertain in range $\Delta = \pm 0.5$ %, referenced to middle point values (nominal, non-perturbed solution). Table 1 shows a sample of detailed results for interval of state variables (node voltage magnitudes and angles), while Table 2 shows the same for interval of output variables (real and reactive branch power flows), obtained by maximized BILF model. The sums of maximum interval widths for different types of state variables are shown in Table 3 for uncertainties in range $\Delta = \pm 0.5$ and ± 1 %.

In addition, we compare our optimization results with a simple, but informative heuristic – an approximate lower bound for a node voltage magnitudes and angles is obtained by considering maximal (PQ + PV)-node real and PQ-node reactive injections, maximal network impedances, and minimal values of measured PV-node voltage magnitudes; the dual case is used for obtaining the approximate upper bound (referred to as "lower/upper bounds" later).

Our results show that maximized BILF model calculates worst-cases of interval results for state variables and other output variables quite effectively. In Figure 2, the results for $\Delta = \pm 0.5$ and ± 1.0 % are compared with those obtained by 20,000 random (Monte Carlo) uniformly distributed, zero-mean variation of input uncertain variables and with heuristic lower/upper bounds approach.

The obtained results suggest that:

1) Maximized BILF model gives useful worst-case bounds.
2) Random (uniformly distributed) variation of network parameters and SCADA measurements (with zero-mean) tends to underestimate the worst-case variations.
3) The variation of input uncertainties has been amplified several times in state and other output variables (as summarized in Table 3).

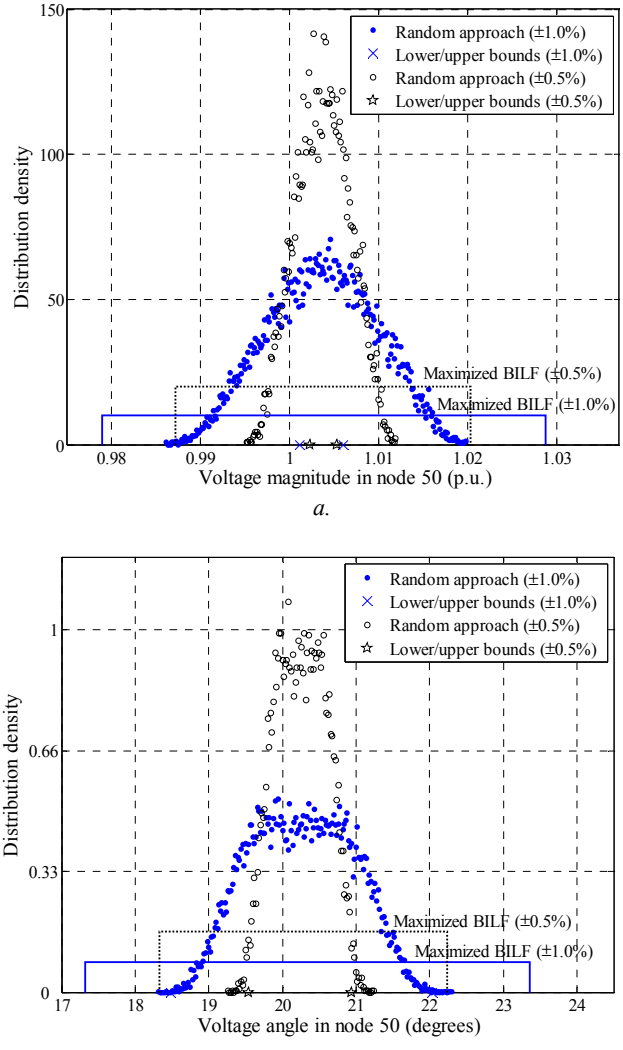

a.

b.

Figure 2: Probability densities in change of solutions (with respect to nominal, non-perturbed case) as a function of random perturbations in SCADA measurements and network branch parameters, compared with maximized BILF solution from Tables 1 and 2 and heuristic lower/upper bounds solution for uncertanty: 1) ±0.5 % and 2) ±1.0 %:

a. Voltage Magnitude in Node 50.

b. Voltage Angle in Node 50.

Node/ Type	Voltage magnitude [low; middle; high] [p.u.]	Voltage angle [low; middle; high] [degrees]	Node/ Type	Voltage magnitude [low; middle; high] [p.u.]	Voltage angle [low; middle; high] [degrees]
1/PQ	[0.977; 1.004; 1.030]	[6.012; 7.433; 8.876]	35/PQ	[0.969; 1.010; 1.052]	[2.388; 3.139; 3.913]
2/PQ	[0.974; 0.986; 0.999]	[6.907; 9.571; 12.240]	36/PQ	[0.929; 0.987; 1.046]	[-0.799;-0.532; -0.266]
3/PQ	[0.954; 0.967; 0.979]	[3.531; 6.161; 8.789]	37/PQ	[0.946; 0.977; 1.008]	[-7.508; -7.050; -6.591]
4/PQ	[0.929;0.943; 0.958]	[2.654; 4.906; 7.155]	38/PQ	[0.980; 1.005; 1.030]	[8.529; 9.695; 10.887]
5/PQ	[0.932; 0.949; 0.965]	[4.002; 5.988; 7.971]	39/PQ	[0.944; 0.975; 1.007]	[-9.690; -8.584; -7.468]
6/PQ	[0.936; 0.952;0.968]	[4.776; 6.751; 8.725]	40/PQ	[1.014; 1.030; 1.046]	[13.444; 16.004; 18.649]
7/PQ	[0.923; 0.941; 0.960]	[2.349; 4.211; 6.071]	41/PQ	[0.989; 0.999; 1.009]	[39.979; 44.964; 50.154]
8/PQ	[0.920; 0.940; 0.960]	[1.804; 3.607; 5.411]	42/PQ	[0.989; 0.999; 1.009]	[32.784; 39.717;46.932]
9/PQ	[0.942; 0.983; 1.025]	[2.350; 3.133; 3.924]	43/PQ	[0.945; 0.976; 1.007]	[-8.645; -7.788; -6.925]
10/PQ	[0.948; 0.961; 0.975]	[7.448; 9.570; 11.687]	44/PQ	[0.945; 0.976; 1.007]	[-8.690;-7.818; -6.938]
...	...	...	...	...	...
33/PQ	[0.973; 1.003; 1.035]	[7.850; 8.546; 9.259]	67/PV	[0.995; 1.000; 1.005]	[33.486; 40.577; 47.957]
34/PQ	[0.963; 1.008; 1.053]	[2.556; 3.175; 3.811]	68/PV	[0.995; 1.000; 1.005]	[43.586; 46.660; 49.877]

Table 1: Node voltage magnitudes and angles obtained by maximized BILF model for New England/New York system.

Branch	Real power flow [low; middle; high] [p.u.]	Reactive power flow [low; middle; high] [p.u.]	Branch	Real power flow [low; middle; high] [p.u.]	Reactive power flow [low; middle; high] [p.u.]
1-2	[-1.085; -0.850; -0.607]	[-0.032; 0.155; 0.384]	26-29	[-1.742;-1.742;-1.742]	[-0.446; -0.291; -0.100]
1-30	[0.895; 1.302; 1.797]	[-0.010; 0.293; 0.594]	28-29	[-3.308;-3.308;-3.308]	[0.060; 0.158; 0.268]
2-3	[3.681; 3.828; 3.989]	[0.940; 0.940; 0.940]	29-61	[-7.909;-7.909;-7.909]	[0.098; 0.489; 0.932]
2-25	[-2.195;-2.195;-2.195]	[0.237; 0.552; 0.894]	9-30	[-3.547;-3.547;-3.547]	[-1.042; -0.491; 0.134]
2-53	[-2.488;-2.488;-2.488]	[-1.059; -0.687; -0.293]	9-36	[2.472; 3.098; 3.839]	[-0.623;-0.623;-0.623]
3-4	[0.696; 0.994; 1.313]	[0.760; 0.893; 0.893]	9-36	[2.472; 3.098; 3.839]	[-0.623;-0.623;-0.623]
...	...	...	...	...	...
26-27	[1.778; 2.501; 3.271]	[0.704; 0.704; 0.704]	52-68	[-39.80;-39.80; -39.80]	[-1.960; -0.255; 1.520]
26-28	[-1.251;-1.251;-1.251]	-0.391; -0.252; -0.086]	1-27	[-0.033; 0.024; 0.102]	[-0.125; -0.123; -0.107]

Table 2: Branch real and reactive power flows obtained by maximized BILF model for New England/New York system.

Non-perturbed (nominal) case			
Input uncertainty [%]	$\sum\lvert\theta_{mi}\rvert$ $(i \in N_{PQ+PV})$ [rad]	$\sum V_{mj}$ $(j \in N_{PQ})$ [p.u.]	$\sum\lvert Q_{mk}\rvert$ $(k \in N_{PV})$ [p.u.]
0.0	15.840	51.023	22.340
Perturbed (uncertain) case			
Input uncertainty [%]	$\sum\Delta\theta_i$ $(i \in N_{PQ+PV})$ [rad]	$\sum\Delta V_j$ $(j \in N_{PQ})$ [p.u.]	$\sum\Delta Q_k$ $(k \in N_{PV})$ [p.u.]
±0.5	5.841	2.041	15.950
±1.0	6.965	3.181	18.588
Relatives			
Input uncertainty [%]	$\frac{\sum\Delta\theta_i}{\sum\lvert\theta_{mi}\rvert}$ [%]	$\frac{\sum\Delta V_j}{\sum V_{mj}}$ [%]	$\frac{\sum\Delta Q_k}{\sum\lvert Q_{mk}\rvert}$ [%]
±0.5	36.875	4.000	71.397
±1.0	43.970	6.234	83.205

Table 3: System-wide comparison of interval widths of power flow solutions for variations in input uncertainties, New England/New York system.

Our quantification of the conservativism of the BILF methodology is illustrated in Figure 3, where we display the range of voltage angle variations in node 50 obtained by extensive Monte Carlo simulations (including non-zero mean parameter variations) and compares it with BILF predictions. From this and numerous other examples we are led to believe that BILF methodology is not excessively conservative.

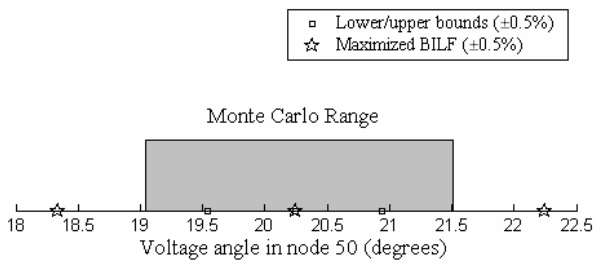

Figure 3: Monte Carlo versus LP predictions, bus 50, 0.5 % perturbation.

Please note that due to the very high order of the problem (approximately 220 unknowns in this example), it is difficult to guarantee that the parameter space

has been adequately "covered" in Monte Carlo simulations; thus, the actual conservativism may well be smaller than the one shown in Figure 3.

5.2 Standard IEEE test system with 300 nodes

The second test system comprises 300 buses, 69 generators and 411 lines. The number of state variables is $2N_{PQ}+2N_{PV}=598$.

The following analyses for different input uncertainties are described in Table 4:

– **Case 1**: Input uncertainties in network data and in measurements:

$$\Delta \boldsymbol{P}_{PQ+PV} = \Delta \boldsymbol{Q}_{PQ} = \Delta \boldsymbol{V}_{PV} = \Delta \boldsymbol{Y}_b^c = \pm 0.5\ \%.$$

– **Case 2:** Measurement uncertainties only:

$$\Delta \boldsymbol{P}_{PQ+PV} = \Delta \boldsymbol{Q}_{PQ} = \Delta \boldsymbol{V}_{PV} = \pm 0.5\ \%.$$

Non-perturbed (nominal) case			
	$\sum\lvert\theta_{mi}\rvert$ $(i \in N_{PQ+PV})$ [rad]	$\sum V_{mj}$ $(j \in N_{PQ})$ [p.u.]	$\sum\lvert Q_{mk}\rvert$ $(k \in N_{PV})$ [p.u.]
	74.295	230.751	74.941
Perturbed (uncertain) case			
Case	$\sum\Delta\theta_i$ $(i \in N_{PQ+PV})$ [rad]	$\sum\Delta V_j$ $(j \in N_{PQ})$ [p.u.]	$\sum\Delta Q_k$ $(k \in N_{PV})$ [p.u.]
1	1.678	6.962	32.548
2	1.544	2.363	31.472

Table 4: System-wide comparison of interval widths of power flow solutions for variations in input uncertainties, IEEE test system with 300 nodes.

As expected, the interval widths are smaller in the second case (when network parameters are fixed). This is particularly true for bus voltage magnitudes. On the other hand, the variations in reactive injections in PV buses are largely determined by measurement uncertainties.

The variation of the (system-wide) sum of interval widths of various quantities (Case 1 in Table 4) as a function of the level of input uncertainty is displayed in Figure 4.

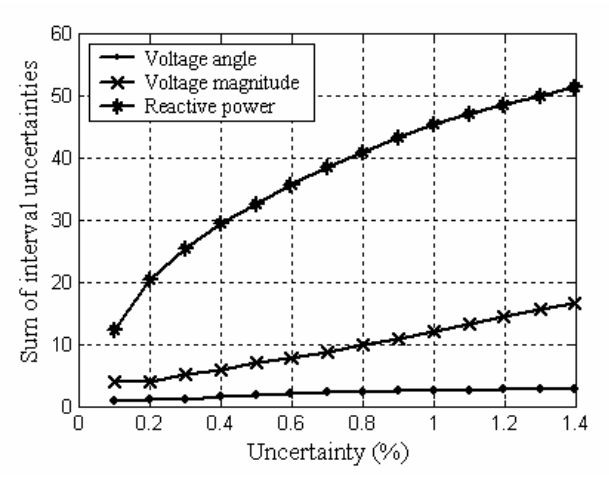

Figure 4: Sum of interval widths of various quantities as a function of the level of input uncertainty (Case 1 in Table 4).

6 CONCLUSIONS

The paper proposes a robust (interval arithmetic and linear programming (LP)-based) method for calculation of worst-cases in power flow analyses with network and measurement data uncertainty. The computational requirements of the proposed method substantially exceed those of standard methods for power flow calculation. However, the information obtained from the algorithm is also much richer, and includes sensitivities to changes in model parameters and in quality of SCADA measurements. In its current state, our implementation is suitable for off-line analyses. We feel that a more streamlined implementation (e.g., with a state-of-the-art LP software like GAMS, and with decoupled power flow) could be capable of solving systems with a few thousands variables, thus potentially opening new application domains.

APPENDIX

BASIC POWER SYSTEM EQUATIONS [11]

The load flow function $\boldsymbol{g}$ (1) written in detailed form for increments in all variables is:

$$\begin{bmatrix} \Delta \boldsymbol{P}_{PQ+PV} \\ \Delta \boldsymbol{Q}_{PQ} \\ \Delta \boldsymbol{V}_{PV} \end{bmatrix} = \begin{bmatrix} \frac{\partial \boldsymbol{P}_{PQ+PV}}{\partial \boldsymbol{\theta}_{PQ+PV}} & \frac{\partial \boldsymbol{P}_{PQ+PV}}{\partial \boldsymbol{V}_{PQ}} & \frac{\partial \boldsymbol{P}_{PQ+PV}}{\partial \boldsymbol{Q}_{PV}} \\ \frac{\partial \boldsymbol{Q}_{PQ}}{\partial \boldsymbol{\theta}_{PQ+PV}} & \frac{\partial \boldsymbol{Q}_{PQ}}{\partial \boldsymbol{V}_{PQ}} & \frac{\partial \boldsymbol{Q}_{PQ}}{\partial \boldsymbol{Q}_{PV}} \\ \frac{\partial \boldsymbol{V}_{PV}}{\partial \boldsymbol{\theta}_{PQ+PV}} & \frac{\partial \boldsymbol{V}_{PV}}{\partial \boldsymbol{V}_{PQ}} & \frac{\partial \boldsymbol{V}_{PV}}{\partial \boldsymbol{Q}_{PV}} \end{bmatrix} \begin{bmatrix} \Delta \boldsymbol{\theta}_{PQ+PV} \\ \Delta \boldsymbol{V}_{PQ} \\ \Delta \boldsymbol{Q}_{PV} \end{bmatrix}, \quad \text{(A1)}$$

where elements of Jacobian matrix are defined for basic injection equations (and calculated for non-perturbed, nominal condition):

$$P_i = V_i^2 G_{ii} + V_i \sum_{k \in \alpha_i} \left[V_k (G_{ik} \cos\theta_{ik} + B_{ik} \sin\theta_{ik}) \right]; \quad \text{(A2)}$$

$$Q_j = -V_j^2 B_{jj} + V_j \sum_{k\in\alpha_j} \left[V_k (G_{jk} \sin\theta_{jk} - B_{jk} \cos\theta_{jk}) \right], \quad \text{(A3)}$$

where:

V_i, θ_i ($\theta_{ik} = \theta_i - \theta_k$) – voltage and phase angle in the i-th node, respectively;

G_{ik}, B_{ik} – elements of bus admittance matrix $\boldsymbol{Y}_{bus}^c = \boldsymbol{G}_{bus} + j\boldsymbol{B}_{bus}$ in position 'ik', respectively; defining, for example, the susceptance part as:

$$B_{ik} = \begin{cases} \sum_{j\in\alpha_i} B_{b,ij} + B_i^{sh}; & i = k; \\ -B_{b,ik}; & i \neq k; \end{cases}$$

α_i – set of nodes connected with i-th node;

B_i^{sh} – sum of shunt susceptances in the i-th node;

$i = 1, 2, \cdots, (n_{PQ} + n_{PV})$; $j = 1, 2, \cdots, n_{PQ}$.

The branch power flow function $\boldsymbol{h}$ (2) contains L-dimensional vectors of real ($\boldsymbol{P}_b$) and reactive power flows ($\boldsymbol{Q}_b$) as parts:

$$\Delta\boldsymbol{P}_b = diag\left\{ \begin{bmatrix} \frac{\partial \boldsymbol{P}_b}{\partial \boldsymbol{\theta}} & \frac{\partial \boldsymbol{P}_b}{\partial \boldsymbol{V}} \end{bmatrix} \right\} \begin{bmatrix} \Delta\boldsymbol{\theta} \\ \Delta\boldsymbol{V} \end{bmatrix}; \quad \text{(A4)}$$

$$\Delta\boldsymbol{Q}_b = diag\left\{ \begin{bmatrix} \frac{\partial \boldsymbol{Q}_b}{\partial \boldsymbol{\theta}} & \frac{\partial \boldsymbol{Q}_b}{\partial \boldsymbol{V}} \end{bmatrix} \right\} \begin{bmatrix} \Delta\boldsymbol{\theta} \\ \Delta\boldsymbol{V} \end{bmatrix}, \quad \text{(A5)}$$

where the derivatives (calculated for non-perturbed, nominal condition) are obtained from following basic branch flow equations:

$$P_{b,ij} = G_{b,ij} V_i^2 - V_i V_j \left(G_{b,ij} \cos\theta_{ij} + B_{b,ij} \sin\theta_{ij} \right); \quad \text{(A6)}$$

$$Q_{b,ij} = -V_i^2 \left(B_{b,ij} + B_i^{sh} \right) - V_i V_j \left(G_{b,ij} \sin\theta_{ij} - B_{b,ij} \cos\theta_{ij} \right). \quad \text{(A7)}$$

REFERENCES

[1] K. Almeida, F. P. Galiana and S. Soures, "A general parametric optimal power flow," *IEEE Trans. on Power Systems*, vol. 9, pp. 540–547, Feb. 1994.

[2] P. R. Gribik, D. Shirmohammadi, S. Hao and C. L. Tomas, "Optimal power flow sensitivity analysis," *IEEE Trans. on Power Systems*, vol. 5, pp. 969–976, Aug. 1990.

[3] P. Zhang and S. T. Lee, "Probabilistic load flow computation using the method of combined cumulants and Gram-Charlier expansion," *IEEE Trans. on Power Systems*, vol. 19, pp. 676–682, Feb. 2004.

[4] L. Xiaoming, C. Xiaohui, Y. Xianggen, X. Tieyuan and L. Huagang, "The algorithm of probabilistic load flow retaining nonlinearity," *Proc. 2002 Power System Technology Conference - PowerCon 2002,* vol. 4, Oct. 2002.

[5] Z. Wang and F. L. Alvarado, "Interval arithmetic in power flow analysis," *IEEE Trans. on Power Systems*, vol. 7, pp. 1341–1349, Aug. 1992.

[6] V. Miranda and J. P. Saraiva, "Fuzzy modeling of power system optimal load flow"*, IEEE Trans. on Power Systems*, vol. 7, pp. 843–849, May 1992.

[7] A. Dimitrovski and K. Tomsovic, "Boundary load flow solutions," *IEEE Trans. on Power Systems*, vol. 19, pp. 348–355, Feb. 2004.

[8] J. W. Chinneck and K. Ramadan, "Linear programming with interval coefficients," *Journal of the Operational Research Society*, vol. 51, pp. 209–220, Feb. 2000.

[9] J. Rohn, "Systems of linear interval equations," *Linear Algebra and its Applications*, vol. 126, pp. 39–78, 1989.

[10] L. Jaulin, M. Kieffer, O. Didrit and É. Walter, *Applied interval analysis.* London, Berlin, Heidelberg: Springer-Verlag, 2001.

[11] A. J. Wood and B. F. Wollenberg, *Power Generation, Operation, and Control.* 2nd ed., New York: Wiley, 1996.